Numerical Simulation of Deflagration to Detonation Process Using Adaptive Mesh Refinement Method in Hydrogen/Oxygen Premixed Gas Mixture: Effect of Flame Shapes

RYU, Yusuke[1] , TSUBOI, Nobuyuki[1] ,
HAYASHI, A. Koichi[2] , OBARA, Tetsuro[3] , TANG, Xin-Meng[4]
[1]Kyushu Institute of Technology
1-1 Sensui, Tobata, Kitakyushu, Fukuoka 804-8550, Japan
[2]Aoyama Gakuin University
Faculty of Engineering, 5-10-1, Futhinobe, Chuo-ku, Sagamihara, Kanazawa, 252-5258, Japan
[3] Saitama University
255 Shimo-Okubo, Sakura, Saitama, Saitama, 338-8570, Japan
[4]International Innovation Center of Tsinghua University, Shanghai, China

1 Introduction

Detonation is a combustion phenomenon sustained by the interaction between a supersonic shock wave in a gas and the associated heating region. Since detonation propagates at supersonic velocities of Mach 4 to 6 and high temperature and pressure, it is important to investigate the mechanism of detonation generation and propagation from the viewpoint of safety engineering. DDT (Deflagration-to-Detonation Transition) is a method of detonation generation. DDT is caused by the growth and acceleration of a turbulent flame, and one of the methods to generate turbulence of a flame is the Shock Flame Interaction (SFI). DDT has been studied extensively in analysis and experiment. In the analysis, Tang et al. [1] performed a numerical simulation of DDT in 2021 by utilizing the AMR method to find three essential conditions for the velocity of the spontaneous reaction wave to transition to DDT. In the study of SFI, Maeda et al. [2] conducted experiments to find that the flame propagation behavior can be roughly classified into four categories depending on the Mach number of the incident shock wave and the distance from the edge wall to the flame front. In the numerical simulations, however, DDT is a complicated phenomenon and the computational cost to investigate the details of DDT is very high. In experiments, it is difficult and expensive to measure detailed transitions of DDT. Therefore, there are still many unresolved aspects of DDT. The adaptive mesh refinement (AMR) method is one of the attractive methods used to reduce computational costs. The AMR method is a numerical technique that reconstructs the computational grid based on the gradient of physical quantities obtained by the analysis. Using this method, DDT's detailed propagation behavior due to SFI can be numerically obtained on a grid with a fine minimum grid width at a lower computational cost than conventional methods. In this study, the effect of different flame shapes of DDT due to SFI in a hydrogen-oxygen premixture is investigated using a two-dimensional numerical analysis by utilizing the AMR method.

Correspondence to: ryu.yusuke438@mail.kyutech.jp

2 Numerical method

Since DDT requires accurate calculation of deflagration, which is affected by diffusion and heat conduction, the Navier-Stokes equations are used in this study. The two-dimensional compressible Navier-Stokes equations with mass conservation for the nine chemical species are used in this study. For the convection term, the AUSMDV scheme [3] with the second-order MUSCL with the minmod limiter is used. For the time integration method, the third-order accurate TVD Runge-Kutta [4] is adopted. The viscosity term is evaluated from the velocity gradient at the cell boundary in the finite volume method. The velocity gradients at the cell boundaries are obtained from the values of neighboring cells, and a second-order accurate central difference method is used. For the chemical reaction model, the Stanford model[5] by Hong et al. which is a detailed chemical reaction model for hydrogen-oxygen gas mixture is used.

For AMR, the Block-AMR code developed by Tang et al. [6] using PARAMESH [7] is adopted. DDT in a tube is caused by the interaction between the shock wave and the boundary layer [8]. Since the resolution of the boundary layer is very important, two AMR blocks are placed on level 9. Each block of guard cells has 8 × 8 grid points. The finest grid width among the nine steps is about 50 [μm] as shown in Eq. (1), and the boundary layer keeps the resolution of 50 [μm] by having two layers of blocks with level 9 of finer grid width near the wall surface.

$$\Delta x = \frac{100}{2^8 \times 8} = 48.8 \times 10^{-3}\ [\mathrm{mm}] = 48.8\ [\mu\mathrm{m}] \qquad (1)$$

Next, it sets the conditions under which the grid is subdivided in the computational domain. The grid is subdivided based on the gradient of the pressure, the temperature, the velocity, and the mass fraction of OH and H_2O_2. Each gradient sets a threshold value for subdivision and de-subdivision of the grid. In this study, the criteria for grid subdivision and de-subdivision are set using absolute differences as follows: pressure: 40/20 [kPa], temperature: 240/120 [K], velocity: 250/100 [m/s], mass fraction of OH: 0.1/0.03, mass fraction of H_2O_2: $1.0\times10^{-8}/1.0\times10^{-9}$, respectively. The calculations were performed on the supercomputer Wisteria of the University of Tokyo with 6 nodes, 48 cores, and 288 processes. Paraview was used to visualize the results. The computation time is approximately 8 to 10 hours.

3 Numerical conditions

Figure 1 shows a present schematic figure of the physical model. The physical model of the computational domain is divided into three regions from the left: Ignition region (IR), Unburned region (UR), and Shock region (SR). The tube size is 100 [mm] in height and 500 [mm] in length, respectively. The incident shock Mach number, M_s, sets 2.03. Table 2 shows the initial conditions in each region for M_s=2.03. For the ignition region, the mass fractions of the premixed gas in the burned state and the adiabatic flame temperature of 2789 [K], which are analyzed in one-dimensional form using the UT-JAXA model [9], are set. The pressure is assumed to be 10 [kPa]. The unburned and shock wave regions are filled with a stoichiometric hydrogen-oxygen premixed gas. The temperature and pressure in the unburned region are 298 [K] and 10 [kPa], respectively. The initial conditions of the shock wave region are obtained from the equations before and after the shock wave as shown in Eq. (2) to (4). The subscripts here are: subscript 1 denotes the unburned region, and subscript 2 denotes the shock wave region. γ is the specific heat ratio, a is the sound velocity, and M_s is the shock wave Mach number. u_p is the flow velocity along the x-axis. Table 3 shows the initial flame shapes. In the SFI experiment, the flame propagation behavior is investigated for different distances x_2 [mm] from the left wall to the flame tip. In this study, the distance from the left wall to the flame tip keeps a constant value and the flame width y [mm] and the length of the parallel part of the flame x_1 [mm] are varied to investigate the difference in flame propagation behavior due to the difference of flame area.

$$\frac{P_2}{P_1} = \frac{2\gamma {M_s}^2 - (\gamma - 1)}{\gamma + 1} \quad (2)$$

$$\frac{T_2}{T_1} = \frac{[2\gamma {M_s}^2 - (\gamma - 1)][(\gamma - 1){M_s}^2 + 2]}{(\gamma + 1)^2 {M_s}^2} \quad (3)$$

$$u_p = \frac{\gamma}{a_1}\left[\frac{P_2}{P_1} - 1\right]\left[\frac{2\gamma}{\frac{P_2}{P_1}(\gamma + 1) + (\gamma - 1)}\right]^{1/2} \quad (4)$$

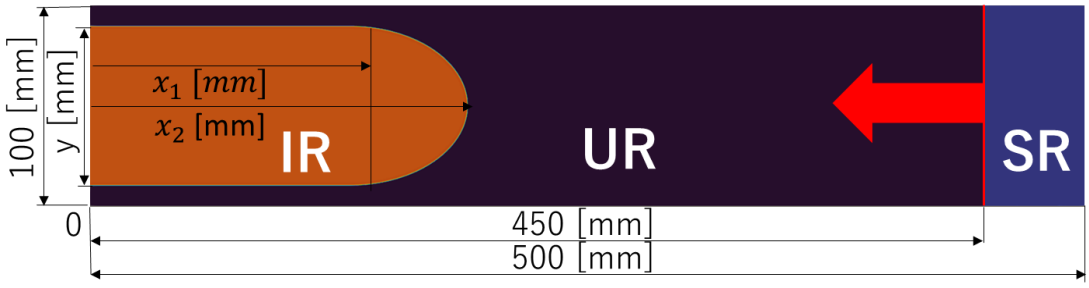

Figure. 1 Schematic of physical model.

Table 2 Initial conditions in each region at M_s=2.03.

Region	Temperature [K]	Pressure [kPa]
Ignition region (IR)	2789	10
Unburned region (UR)	298	10
Shock region (SR)	520	47

Table 3 Flame shape.

Case	y [mm]	x_1 [mm]	x_2 [mm]	Flame area [mm^2]
1	67.4	130.5	190	11940
2	80.0	0		11940
3		130.5		14180
4	95.0	0		14180
5		130.5		16840

4 Results and discussion

4.1 Inflow of unburned gas at interaction between flame and shock wave

Figure 2 shows the incident shock waves in Cases 1 and 2, from the time at the arriving the incident shock wave to the burned area to the time the shock wave was reflected to the left wall. In (a) to (c), the upper half shows the density gradient, and the lower half shows the Mach number distribution, where IS is the incident shock wave and RS is the reflected shock wave. In Fig. 2(a), the incident shock wave interacts with the flame. In Fig. 2(b), the incident shock wave propagates in the unburned region and the ignition region, however, the shock wave propagates faster in the burned gas region than in the unburned region because of the higher temperature in the burned gas region. In Fig. 2(c), unburned gas flows into the combustion gas because of the Meshkov instability caused by the interference of the incident shock

wave. The incident shock wave becomes a reflected shock wave at the left wall and propagates toward the right. The Richtmyer-Meshkov instability is a phenomenon in which a high-density fluid flows into a low-density fluid when a shock wave impinges on a curved contact surface. In this case, it is considered that the shock wave impinges on the curved burned gase and that the high-density unburned gas flows into the low-density burned gas, resulting in instability at the contact surface. Here, the unburned gas flows into Case 2 more clearly than into Case 1. This indicates that the unburned gas flows into the flame more clearly when the curvature of the flame surface is larger, even when the distance from the left wall to the flame tip is the same. The same tendency was observed in other cases.

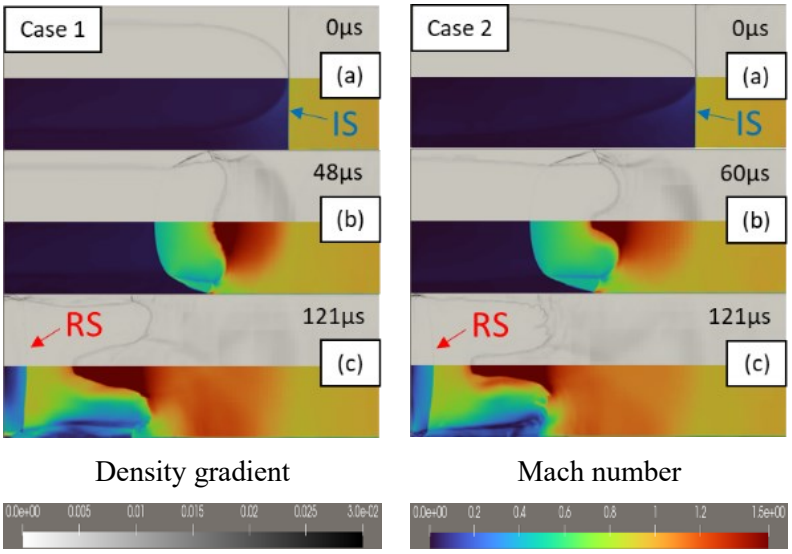

Figure. 2 Incident shock wave interference with flame in Case 1 and Case 2.

4.2 Processes to generate a local explosion

Figure 3 shows the propagation behavior of the reflected shock wave and flame in Cases 1 to 5. In Fig. 3(d) to (g), the upper half of the figure shows the density gradient and the lower half of the figure is the Mach number distribution, where IS is the incident shock wave, RS is the reflected shock wave, and BS is the branching shock wave, respectively. In Fig. 3(d), the reflected shock wave impinges on the unburned gas and propagates in the burned gas. Then, in Fig. 3(e), the reflected shock wave propagates along the flame surface. Comparing the flame shapes, similar flame shapes are observed in Cases 1 and 2, and Cases 3 and 4, respectively. This is because the burned gases are compressed by the incident shock wave, and the change in the flame shape is smaller than that in cases 1 to 4 in Fig. 3. Fig. 3(f) shows that the flame propagates in the boundary layer behind the reflected shock wave for Cases 1 to 4. In Case 5, the flame propagates without separating from the reflected shock wave and forms a bifurcated shock wave. In Fig. 3(g), the flame catches up with the reflected shock wave to become a bifurcated shock wave for Cases 1 to 4. In all cases, a local explosion appears behind the shock wave, and the deflagration transitions to the detonation. Fig. 3(e) to (g) shows that the processes of Cases 1 and 2, and Cases 3 and 4 are similar features. Therefore, when the distance between the left wall and the flame tip is approximately constant, the process to become the detonation is considered to be more affected by the flame area than by the curvature and flame width.

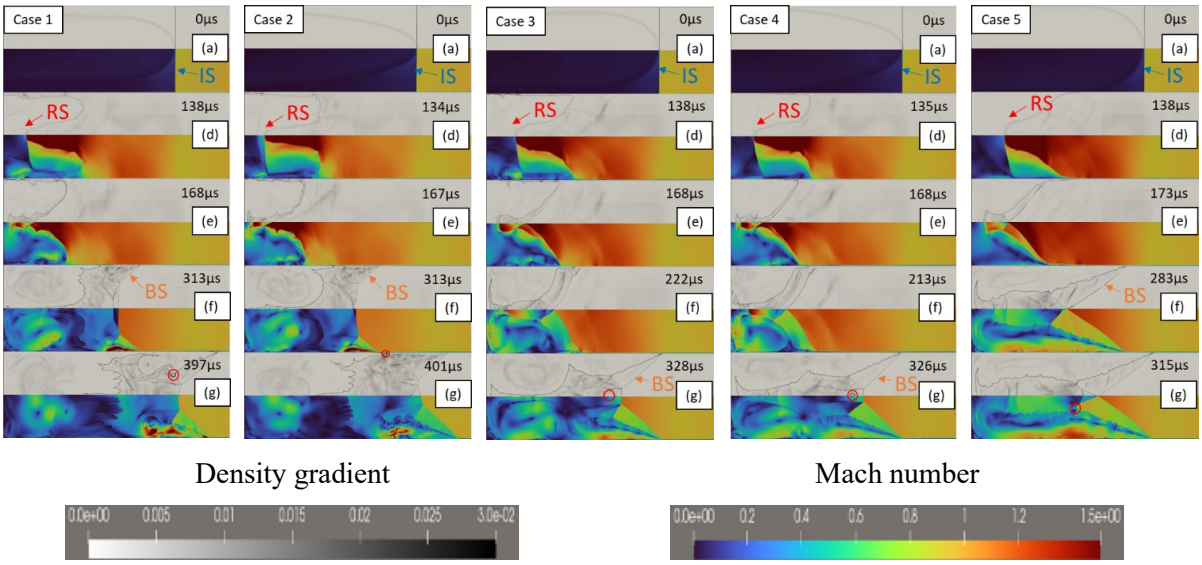

Figure. 3 The propagation behavior of the reflected shock wave and flame in Cases 1 to 5.

5 Conclusions

In this study, numerical simulations on the DDT process with the interaction between the shock wave and the flame in oxygen-hydrogen premixed gas are performed to find the following results:

・As the curvature of the initial flame increases, the inflow of unburned gas due to the interaction with the incident shock waves clearly understood.

・The inflow feature of unburned gases after interacting with the incident shock wave depends on the curvature of the initial flame. However, the effect of its curvature becomes small after the incident shock wave compresses the flame.

・The initial flame area affects the process of the onset of the explosion after the reflected shock wave passes through the unburned gas.

Acknowledgments

This study was carried out using the Wisteria-O at the University of Tokyo. The authors would like to appreciate the Information Technology Center at the University of Tokyo.

References

[1] Tang, X., Dzieminska, E., Hayashi, A. K. and Tsuboi, N., International Journal of Hydrogen Energy, Vol. 46, 2021.

[2] Maeda, S., Kuramochi, Y., Ono, R. and Obara, T., Transactions of JSME, Vol. 83, No. 850, 2017.

[3] Liou MS, Wada Y., AIAA Paper, 94-0083, 1994.

[4] Gottlieb S, Shu CW, Tadmor E., SIAM Review, Vol. 43(1), pp 89-112, 2001.

[5] Hong ZK, Davidson DF, Hanson RK., Combust Flame, pp 633-44, 2011.

[6] Tang XM, Asahara M, Hayashi AK, Tsuboi N., International Journal of Hydrogen Energy, pp 7120-34, 2017.

[7] MacNeice P, Olson KM, Mobarry C, de Fainchtein R, Packer C., Computer Physics Communications, Vol. 125(3), pp 330-54, 2000.

[8] Dzieminska, E. and Hayashi, A. K., International Journal of Hydrogen Energy, 38, pp 4185-4193, 2013.

[9] Shimizu, K., Hibi, A., Koshi, M, Morii, Y. and Tsuboi, N. JOURNAL OF PROPULSION AND POWER, 27(2), pp 383-395, 2011.